Taylor & Francis
Taylor & Francis Group

A perovskite solar cell-photothermal-thermoelectric tandem system for enhanced solar energy utilization

Han Zhong[a]*, Yangying Zhou[a,b]*, Cong Wang[c], Chunlei Wan[a], Kunihito Koumoto[d], Zhiping Wang[e,f] and Hong Lin[a]

[a]State Key Laboratory of New Ceramics & Fine Processing, School of Materials Science and Engineering, Tsinghua University, Beijing, China;
[b]Huaneng Clean Energy Research Institute, Beijing, China;
[c]School of Integrated Circuit Science and Engineering, Beihang University, Beijing, China;
[d]Nagoya Industrial Science Research Institute, Nagoya, Aichi, Japan;
[e]School of Physics and Technology, Hubei Luojia Laboratory, Key Lab of Artificial Micro- and Nano-Structures of Ministry of Education, School of Microelectronics, Wuhan University, Wuhan, China;
[f]Wuhan Institute of Quantum Technology, Wuhan, China

ABSTRACT

Photovoltaic-thermoelectric (PV-TE) tandem system has been considered as an effective way to fully utilize the solar spectrum, and has been demonstrated in a perovskite solar cell (PSC)-thermoelectric (TE) configuration. However, the conventional PSC-TE tandem architecture cannot convert infrared light transmitted through the upper PSC into heat effectively, impeding the heat-electricity conversion of TE devices. Herein, a semi-transparent PSC-photothermal-TE tandem system is designed for improved photothermal utilization. Through optimizing the buffer layer of the back transparent electrode, semi-transparent PSC with a power conversion efficiency (PCE) of 13% and an average transmittance of 53% in the range of 800–1500 nm was obtained. On this basis, a photothermal thin film was introduced between the semi-transparent PSC and the TE device, which increased the efficiency contribution ratio of the TE device from 14% to 19%, showing enhanced utilization of AM 1.5 G solar spectrum and improved photo-thermal-electric conversion efficiency.
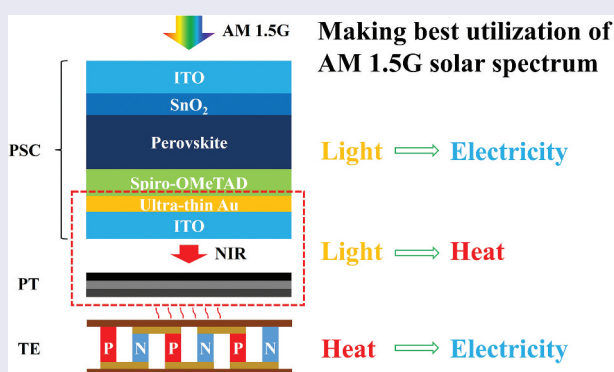
IMPACT STATEMENT

We have constructed a semi-transparent perovskite solar cell-photothermal-thermoelectric tandem system through the optimization of transparent back electrode and the introduction of photothermal thin-film, realizing enhanced utilization of solar energy.

1. Introduction

Nowadays, with the energy and environmental issues become increasingly prominent, clean energy represented by photovoltaic and wind power has gradually received more widespread attention. Therein, the utilization of solar energy with abundant reserves is considered to be a key technology. Solar energy utilization can be mainly divided into two categories, photovoltaic and photothermal. Photovoltaic devices have flexible and wide applications, but their power conversion efficiency (PCE) is limited. While for

photothermal devices, although with high PCE, their application scenarios are relatively few [1]. Therefore, the development of high-quality light-thermal-electric multi-energy coupling devices has attracted increasing research interest.

For photovoltaic devices, owing to the excellent photoelectric performance of metal-halide perovskite materials, including high absorption coefficient [2], high carrier mobility [3], and long carrier diffusion length [4], perovskite solar cells (PSCs) have attracted extensive attention and experienced a rapid development in the past decade. At present, the PCE of single-junction PSCs has reached 26.1%, with the PCE of perovskite/silicon tandem solar cells reaching 33.9% [5]. However, PSCs are sensitive to light, humidity, and heat, resulting in insufficient long-term stability, impeding their practical application. A promising way to solve this problem is combining PSCs with thermo-electric (TE) devices to construct PSC-TE tandem systems, which can not only improve the power output and PCE, but also reduce the operating temperature and waste heat emission.

In recent years, attention to photovoltaic-thermoelectric (PV-TE) tandem systems has increased globally, but the overall research is still insufficient. Most of the studies focused on theoretical simulation, mainly based on different theoretical simulation methods and tandem models, to study the impact of photovoltaic materials, device geometric parameters, device structure, etc., on the temperature distribution, PCE, and other performance of PV-TE tandem system [6–8]. Researchers showed that organic photovoltaic materials can play a greater role in the development of PV-TE tandem system [9]. No matter for dye-sensitized solar cells (DSSCs), organic photovoltaics (OPVs) or PSCs, the introduction of thermoelectric devices can achieve a large increase in open circuit voltage (V_{oc}) and PCE [10]. Chang et al. used electrophoretic deposition to deposit CuO nanofluids on a copper plate and adhere to the surface of TE, thereby enhancing the overall heat conduction of the device, increasing the temperature difference between the thermoelectric ends by about 2°C, increasing the thermoelectric conversion efficiency by about 10% and increasing the total power output by 2.4% [11]. For PSCs, Liao et al. established a theoretical model of the PSC-TE tandem system and proposed that when the thickness of the perovskite layer is 449.7 nm and the device area is 3.24×10^{-2} m^2, the maximum tandem efficiency can reach 22.9% [12]. Fu et al. prepared a 16 cm^2 perovskite solar module (PSM)-thermoelectric tandem device, and the optimal PSM-TE tandem device efficiency reached 12.7% [13]. Our research team also carried out a series of investigations on PSC-TE tandem systems, with the highest PCE exceeding 25% [14,15].

In order to improve the photothermal utilization of PV-TE tandem devices, researchers have made many attempts. Liu, Xu et al. both prepared a carbon counter electrode-based PSC-TE tandem system, using carbon electrode as the infrared light absorption layer of the thermoelectric device, but the overall device efficiency is still relatively low [16,17]. In Liu's research, although the output voltage of thermoelectric device was increased by three times, the overall PCE was only increased from 9.9% to 12.6%. Wang et al. introduced a photothermal film into the DSSC-TE tandem to achieve efficient photothermal conversion in visible and near-infrared (NIR) regions, and the device efficiency was significantly improved. Compared with single DSSC, the efficiency of tandem device increased about 50%, which reached 13.8%, proving that improved photothermal utilization of the tandem device can effectively improve the device performance [18].

In this work, efficient semi-transparent perovskite solar cells (STPSCs) with good NIR transmittance were realized by the adoption of indium tin oxide (ITO) back transparent electrode and ultra-thin Au buffer layer. Subsequently, we designed a semi-transparent perovskite solar cell-photothermal thin-film-thermoelectric (STPSC-PT-TE) tandem architecture. By introducing the photothermal thin-film, infra-red light transmitted through the upper STPSC can be fully absorbed and converted into heat, which can be utilized by the lower thermoelectric device, delivering a high-quality light-thermal-electric multi-energy coupling device. The tandem device shows improved solar energy utilization, with good operational stability meanwhile. Our work proves the feasibility of the comprehensive utilization of solar energy, which lays a good foundation for the development of new structure and high efficiency utilization of solar energy.

2. Experimental details

2.1. Materials

Tin(IV) oxide nanoparticles (15 wt% dispersed in deionized water), lead iodide (PbI$_2$, 99.999%), cesium iodide (CsI, 99.999%), lead bromide (PbBr$_2$, 99.998%), N,N-dimethylformamide (DMF, anhydrous, 99.9%), and chlorobenzene (CB, 99.9%) were bought from Alfa Aesar. Formamidinium iodide (FAI, 99%) and methylammonium bromide (MABr, 99%) were purchased from Greatcell Solar. Spiro-OMeTAD (99.7%) was purchased from Lumtech. Acetonitrile (99.9%) was purchased from J&K Scientific. Dimethyl sulfoxide (DMSO, anhydrous, 99.9%), bis(trifluoromethane) sulfonamide lithium salt (Li-TFSI, 99.95%), and 4-tert-butyl pyridine (t-BP, 96%) were supplied by Sigma-Aldrich. Methylamine chloride (MACl, 99.5%), octylammonium iodide (OAI, 99.5%), and FK209 Co(III) TFSI salt (99.0%) were purchased from Xi'an Polymer

Light Technology Co., Ltd. All the chemical reagents were used as received without further purification. The ITO glasses (7 Ω/sq) were purchased from Advanced Election Technology Co., Ltd. The thermoelectric generator (TE, XH-F241A1126) was produced by Xinghe Electronic Technology and was used as purchased. The detailed performance of this commercial TE is shown in Table S1. The cooling system used a LX-1000 Coolium water cooling circulator.

2.2. *Device fabrication*

The ITO glasses were cleaned in a sequence of detergent, ultrapure water, ethanol, acetone, and isopropanol with 15 min ultra-sonication for each step. Before the deposition of electron-transport layer, the substrates were treated with oxygen plasma for 15 min. SnO_2 electron-transport layer was fabricated by spin-coating the solution of Tin(IV) oxide nanoparticles (2.5 wt%, diluted in deionized H_2O) at 4000 rpm for 30 s, and annealed at 120°C for 40 min. Before the deposition of perovskite layer, they were treated with oxygen plasma for 2 min. The $Cs_{0.05}(FA_{0.9}MA_{0.1})_{0.95}Pb(I_{0.9}Br_{0.1})_3$ precursor solution, at a concentration of 1.4 M, was prepared by mixing CsI, FAI, MABr, PbI_2 and $PbBr_2$ in molar ratio in an anhydrous DMSO/DMF mixture with a volume ratio of 1:9, 30% additional MACl was added in order to optimize the crystallization process. The perovskite layer is deposited using the one-step spin-coating technology (1000 rpm for 10 s and 4000 rpm for 45 s), with chlorobenzene quickly dropped onto the center at 8–10 s before the end of the spinning process. The perovskite layer was then annealed at 100°C for 30 min. 90.0 mg Spiro-OMeTAD powder was dissolved in 1 mL chlorobenzene, with the addition of 39.0 μL tBP, 23.0 μL Li-TFSI (520 mg/mL in acetonitrile) and 10 μL FK-209 Co(III)TFSI (375 mg/mL in acetonitrile) Note that the solution should be thoroughly mixed and let stand for at least 1 h before using. The Spiro-OMeTAD precursor solution was then spin-coated at 4000 rpm for 40 s. Then, the samples were kept in a dry box overnight for oxidation. For back transparent electrode, ITO with a thickness of 300 nm was deposited by radio frequency magnetron sputtering. ITO electrodes were sputtered at 90 W with the Ar flow rate of 6.55 sccm. The base pressure was 1.0×10^{-4} Pa and the working pressure was maintained at 0.35 Pa. For ultra-thin Au buffer layer, ~5 nm Au was deposited by thermal evaporation under a vacuum of 1×10^{-4} Pa. The electrical series structure was established by soldering the Au anode of PSC and the negative pole of TE. For lower heat conduction loss, thermal conductive adhesive was used between PSC and TE in a PSC-TE tandem system, and between photothermal (PT) thin-film and TE in a STPSC-PT-TE system.

2.3. *Characterization*

Transmission spectra were recorded with a Lambda 950 spectrophotometer (PerkinElmer, U.S.A.) at room temperature. The surface morphology of thin-film and cross section of PSC were observed with the scanning electron microscope (SEM, LEO1530, Zeiss, Germany). The crystal structures of thin films were obtained by an X-ray diffractometer (D8 Advance, Bruker, German) with Cu Kα (λ = 1.5406 Å) radiation. The photocurrent density-voltage (*J-V*) characteristics of PSCs, TE, and tandem systems were measured with a digital source meter (2400, Keithley Instruments, U.S.A.) under AM 1.5 G illumination (100 mW/cm) by a solar simulator (91192, Oriel, U.S.A.) calibrated with a standard crystalline silicon solar cell. The active area of the single PSCs and the tandem systems were both 0.06 cm^2. During all the *J-V* measurements, the environment temperature was maintained at 25°C, and the temperature of cooling system was set at 5°C. The monochromatic incident photon-to-electron conversion efficiency (IPCE) was measured by a solar cell quantum efficiency measurement system (QEX10, PV measurements, U.S.A.). The intensity of incident monochromatic light was calibrated with a standard silicon solar cell (1H020, PV Measurements, U.S.A.) in DC mode. Electrochemical impedance spectroscopy (EIS) was measured using a Zahner system (Zahner, Zahner-Electric GmbH & Co., KG, Germany). EIS was recorded at a bias of 0.9 V with a modulation amplitude of 10 mV at frequencies ranging from 1 Hz to 1 MHz in the dark. The temperature distribution and interface temperature of devices were measured with infrared imaging device (TIS75, Fluke, U.S.A.) and K-type thermocouple (SMPW-TT-K- 30-SLE, OMEGA, U.S.A.).

3. Results and discussions

3.1. *Optimization of STPSC*

For a STPSC-PT-TE tandem system, the overall power output is decided by the output of both STPSC and TE. Therefore, besides the PCE itself, the NIR transmittance of STPSC is also essential, since it determines the utilization of NIR light by the lower PT and TE. Here, ITO was selected as the back transparent electrode to fulfill the need of NIR transmittance. Considering the limitations of thermal stability of perovskite and charge-transport layers, ITO thin-films were prepared by radio frequency (RF) magnetron sputtering at room temperature. However, ITO thin-film showed unclear grains morphology (Figure 1(a)), which could be attributed to the low
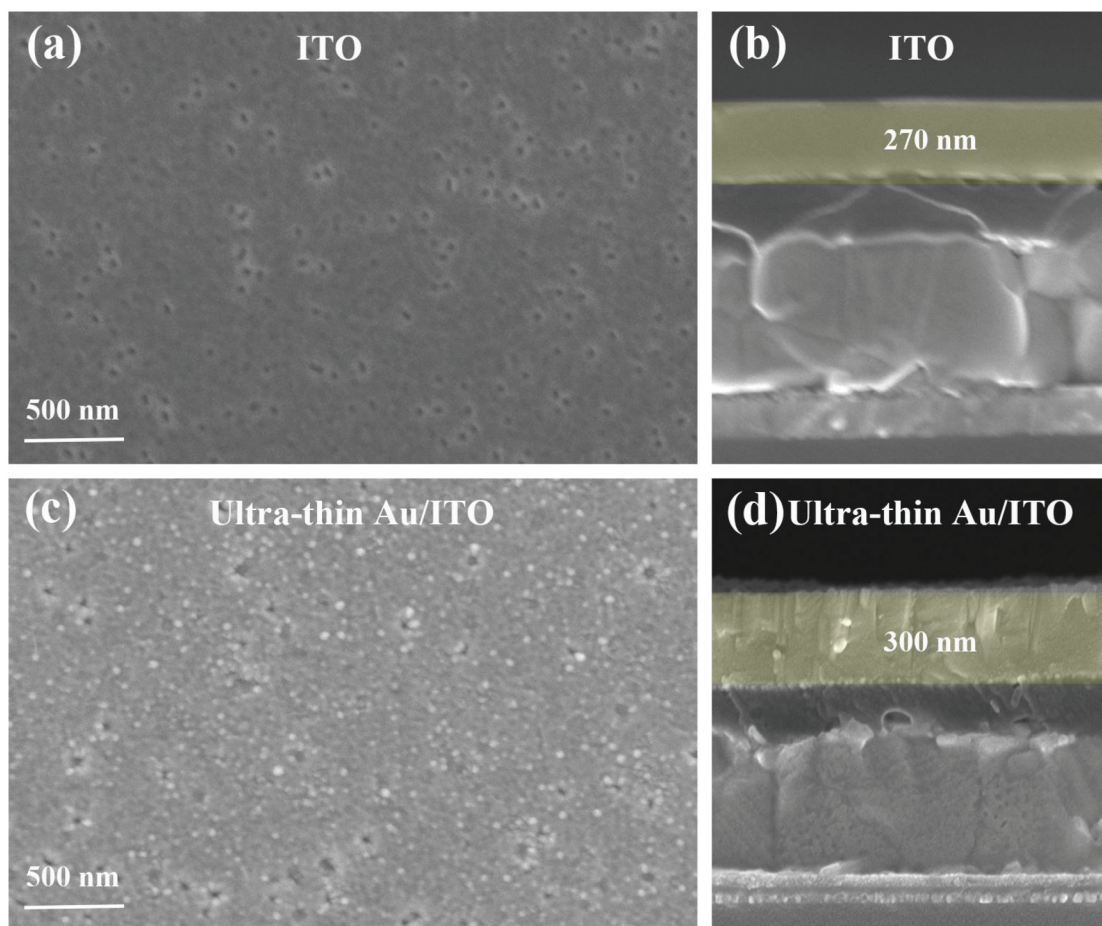
Figure 1. Surface SEM image of (a) ITO and (c) Ultra-thin Au modified ITO. Cross-sectional SEM image of STPSCs based on (b) ITO and (d) Ultra-thin Au modified ITO.

sputtering temperature. Meanwhile, although the sputtering power was reduced, direct sputtering of ITO still caused certain damage to the lower hole-transport layer. Pin-holes can be clearly observed at the interface between the electrode and transport layer (Figure 1(b)), which is unfavorable for charge transfer and collection, thus lowering the PCE of STPSCs and the tandem system.

To address these issues, an ultra-thin Au layer was pre-deposited as a buffer layer. After the introduction of an ultra-thin Au buffer layer, ITO thin-films showed uniform and dense grains on the surface (Figure 1(c)), with a complete columnar structure from the cross-section (Figure 1(d)). Meanwhile, we observe increased intensity for all diffraction peaks, suggesting enhanced crystallinity (Figure 2(a)). From the cross-sectional SEM image (Figure 1(d)), the pin-holes at interface disappeared, indicating that the buffer layer can effectively reduce the damage on the lower layer caused by the sputtering process.

Subsequently, STPSCs based on different ITO back transparent electrodes were prepared. From the J-V curves of STPSCs (Figure 2(b)), compared to directly-sputtered ITO electrodes, the introduction of an ultra-thin Au buffer layer results in a small increase in short-circuit current density (J_{sc}) and a significant

increase in fill factor (FF). With the barely changed V_{oc}, PCE has been increased to 13.4%. This is mainly due to the good conductivity of Au, as well as the significantly improved charge transfer and collection at the interface. From the EIS results (Figure 2(c)), typical semicircle in the high-frequency region has been observed in the Nyquist plot, which represents the series and contact resistance (R_{CT}) of PSCs. The fitting results show that, the R_{CT} decreased from 6237 Ω to 4835 Ω after the introduction of the ultra-thin Au buffer layer, indicating improved charge transfer process. Meanwhile, the STPSC based on ultra-thin Au modified ITO showed an average transmittance of 53.0% in the NIR region of 800–1500 nm (Figure 2(d)), demonstrating good infrared transmittance at the device level.

3.2. Construction of STPSC-PT-TE tandem system

Based on the optimized STPSCs described above, STPSC-TE tandem system was constructed, and PT thin-film was introduced between STPSC and TE for architecture optimization, as shown in Figure 3(a). The schematic diagram of the structure of the PT thin-film is shown in Figure 3(b). The PT thin-film with a metal/ceramic multi-layer structure can reduce its
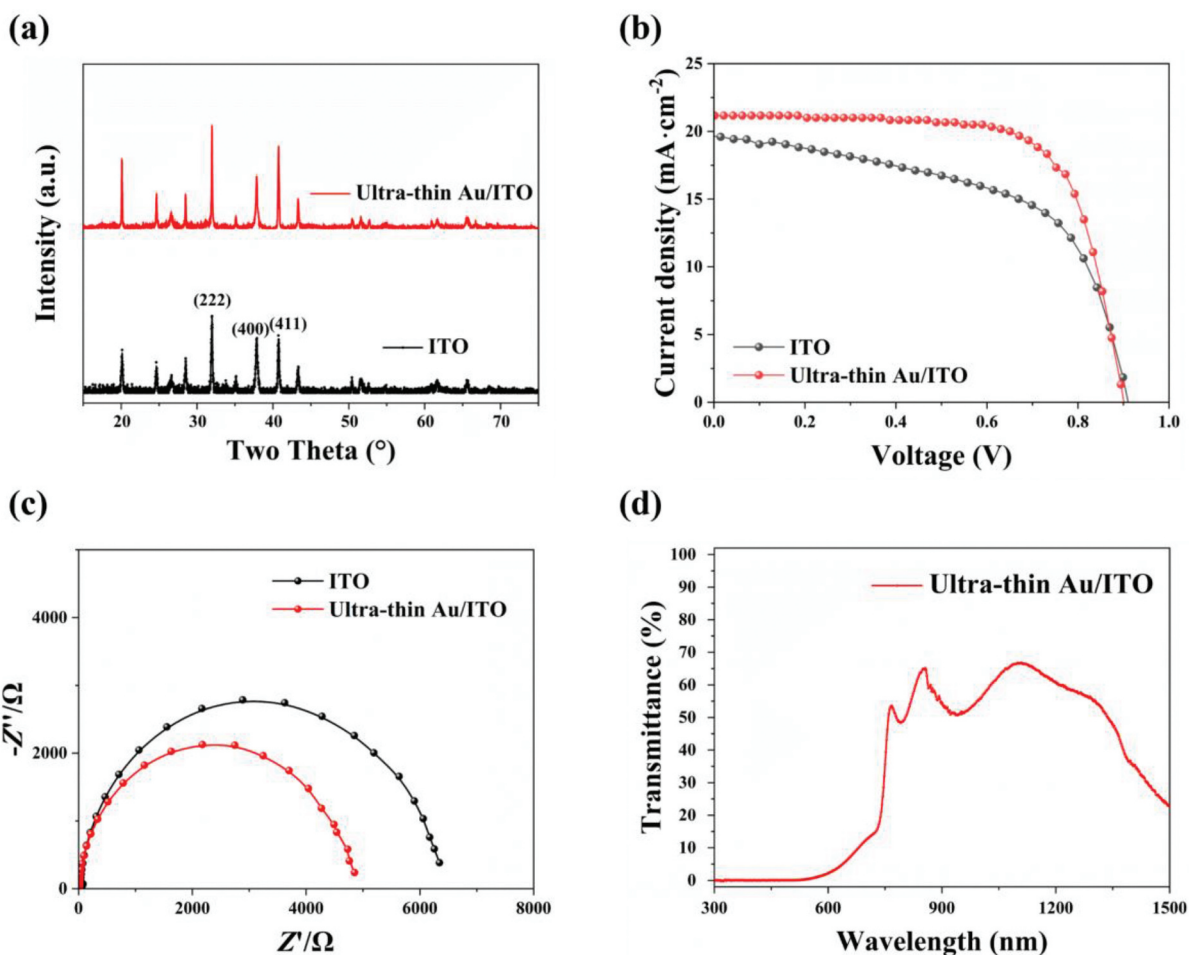
Figure 2. (a) X-ray diffraction patterns of different ITO thin-films. (b) *J-V* curves of STPSCs based on different ITO electrodes. (c) EIS spectrum of STPSCs based on different ITO electrodes. (d) Transmittance of STPSC based on ultra-thin Au-modified ITO.
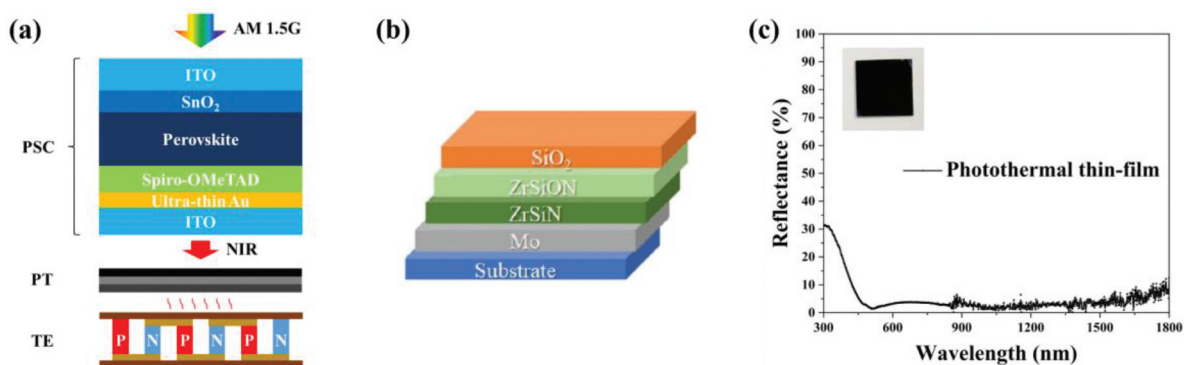

Figure 3. The structural illustration of STPSC-PT-TE tandem system. (a) The structural illustration (b) and reflectance (c) of the PT thin-film.

reflectivity in the infrared region by adjusting the thickness of layers, thus achieving higher light absorption and lower thermal emissivity. The reflectivity of the PT thin-film in the visible and NIR region was tested, as shown in Figure 3(c). In the wavelength range of 300–1800 nm, the average reflectivity of the film was only 5.1%, and the light absorption rate was close to 95%. At 80°C, the thermal emissivity of the film was less than 7%, demonstrating good spectral selective absorption performance and photothermal conversion performance in the visible and NIR region.

Figure 4(a) shows the infrared thermal image of the tandem device in the vertical illumination direction, and the corresponding sectional temperature distribution is shown in Figure 4(b). After the introduction of the PT thin-film, although the average operating temperature of the STPSC is basically unchanged, the temperature difference between the upper and lower
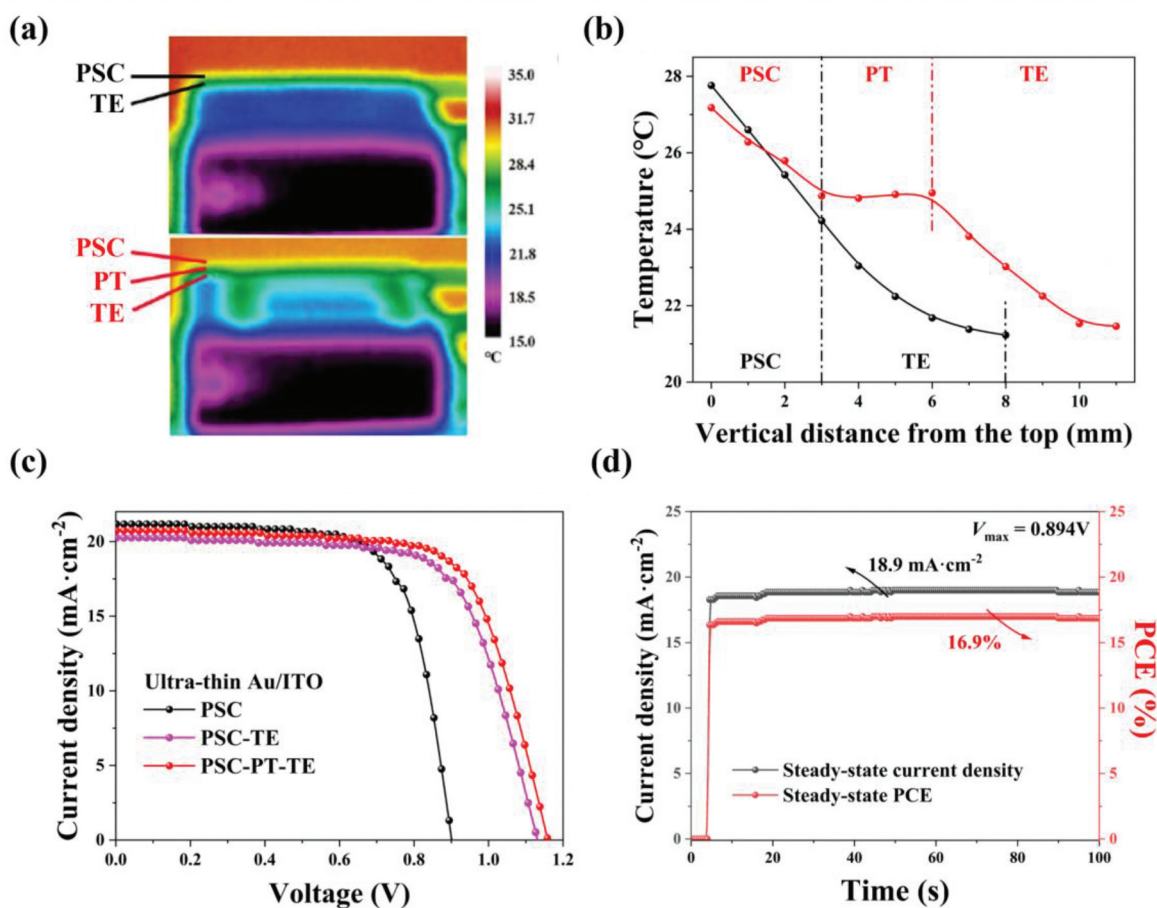
Figure 4. Cross-sectional infrared thermal image (a) and temperature distribution (b) of the STPSC-PT-TE tandem system. (c) *J-V* curves of STPSC, STPSC-TE tandem, and STPSC-PT-TE tandem under standard illumination. (d) Steady-state current density and PCE of STPSC-PT-TE tandem at maximum power point.

sides of the TE increased from 3.0°C to 3.5°C, due to the high infrared transmittance of the upper STPSC and the excellent photothermal conversion performance of PT thin-film. These results indicate that the introduction of PT thin-film can effectively improve the comprehensive utilization of light and heat of the device, and thus improve the thermoelectromotive force and power output of the TE in the tandem device.

From the *J-V* curve of the STPSC and tandem devices (Figure 4(c)), the J_{sc} and FF decreased slightly after the construction of STPSC-TE tandem, which can be attributed to the small increase in the contact resistance or series resistance due to electrical connection. However, the V_{oc} of the device is significantly improved. After the introduction of PT thin-film, the temperature difference between the upper and lower sides of TE can be increased from 6.8°C to 8.2°C. Note that these temperatures are measured by a thermocouple placed at the center of the devices, which might be a slightly different from the values obtained by the infrared thermal image. As a result, the thermoelectromotive force of the TE increased from 0.23 V to 0.27 V, which contributes 19% to the PCE of the tandem device. By contrast, in a PSC-TE

tandem with Au back electrode-based PSC of the same perovskite composition, the thermoelectric temperature difference at both ends is only 7.1°C, and the thermoelectric efficiency contribution ratio is only about 13%, as reported in our previous work [14]. These results further prove that the introduction of PT thin-film can effectively improve the comprehensive utilization of light and heat of tandem devices, realizing the efficient conversion of light-heat-electricity in the NIR region.

Figure 4(d) tracks the steady-state current change of STPSC-PT-TE tandem device under the maximum power point bias. With the extension of illumination time, the device gradually reaches the thermal equilibrium state. The steady-state current density increases slightly, reaching 18.9 mA/cm², and the steady-state PCE reaches 16.9%. The track of steady-state shows that after the introduction of PT thin-film, the tandem device also has good operational stability under illumination.

4. Conclusions

In conclusion, we purposed a STPSC-PT-TE tandem system enabling by the optimization of back

transparent electrode and the introduction of PT thin-film, realizing efficient utilization of solar radiation through comprehensive utilization of light and heat. For ITO back transparent electrodes, ultra-thin Au layer was developed as a buffer layer, which improved the interface quality and crystallinity of ITO. STPSC showed an average transmittance of 53.0% at NIR region, and a PCE of 13.4%. Compared to the PSC-TE tandem based on PSC with Au back electrode, the construction of STPSC-PT-TE tandem improved the temperature difference of TE from 7.1°C to 8.2°C, with the PCE contribution of TE increased from 14% to 19%. This work shows that the architecture design of STPSC-PT-TE tandem can optimize the distribution of spectrum and increase the comprehensive light-heat-electricity conversion efficiency in NIR region, realizing efficient utilization of solar energy.

Disclosure statement

The corresponding author Hong Lin is an Associate Editor for *Science and Technology of Advanced Materials* and was not involved in the editorial review or the decision to publish this article.

Funding

References

[1] Heremans JP, Dresselhaus MS, Bell LE, et al. When thermoelectrics reached the nanoscale. Nature Nanotechnol. 2013;8(7):471–473. doi: 10.1038/nnano.2013.129

[2] De Wolf S, Holovsky J, Moon SJ, et al. Organometallic halide perovskites: sharp optical absorption edge and its relation to photovoltaic performance. J Phys Chem Lett. 2014;5(6):1035–1039. doi: 10.1021/jz500279b

[3] He YP, Galli G. Perovskites for solar thermoelectric applications: a first principle study of $CH_3NH_3Al_3$ (A = Pb and Sn). Chem Mater. 2014;26(18):5394–5400.

[4] Stranks SD, Eperon GE, Grancini G, et al. Electron-hole diffusion lengths exceeding 1 micrometer in an organometal trihalide perovskite absorber. Science. 2013;342(6156):341–344. doi: 10.1126/science.1243982

[5] Best research-cell efficiencies [Internet]. National Renewable Energy Laboratory; [cited 2024 Feb 8]. Available from: https://www.nrel.gov/pv/celleffi ciency.html

[6] Kraemer D, Hu L, Muto A, et al. Photovoltaic-thermoelectric hybrid systems: a general optimization methodology. Appl Phys Lett. 2008;92(24). doi: 10.1063/1.2947591

[7] van Sark W. Feasibility of photovoltaic - thermoelectric hybrid modules. Appl Energy. 2011;88 (8):2785–2790. doi: 10.1016/j.apenergy.2011.02.008

[8] Vorobiev Y, González-Hernández J, Vorobiev P, et al. Thermal-photovoltaic solar hybrid system for efficient solar energy conversion. Sol Energy. 2006;80 (2):170–176. doi: 10.1016/j.solener.2005.04.022

[9] Tvingstedt K, Deibel C. Temperature dependence of ideality factors in organic solar cells and the relation to radiative efficiency. Adv Energy Mater. 2016;6(9). doi: 10.1002/aenm.201502230

[10] Günes S, Neugebauer H, Sariciftci NS. Conjugated polymer-based organic solar cells. Chem Rev. 2007;107(4):1324–1338. doi: 10.1021/cr050149z

[11] Chang H, Kao MJ, Cho KC, et al. Integration of CuO thin films and dye-sensitized solar cells for thermoelectric generators. Curr Appl Phys. 2011;11(4):S19–S22. doi: 10.1016/j.cap.2010.12.039

[12] Liao TJ, He QJ, Xu QD, et al. Performance evaluation and optimization of a perovskite solar cell-thermoelectric generator hybrid system. Energy. 2020;201. doi: 10.1016/j.energy.2020.117665

[13] Fu P, Qin W, Bai S, et al. Integrating large-area perovskite solar module with thermoelectric generator for enhanced and stable power output. Nano Energy. 2019;65. doi: 10.1016/j.nanoen.2019.104009

[14] Zhou Y, Yin X, Zhang Q, et al. Perovskite solar cell-thermoelectric tandem system with a high efficiency of over 23%. Mater Today Energy. 2019;12:363–370. doi: 10.1016/j.mtener.2019.03.003

[15] Zhou Y, Chen Y, Zhang Q, et al. A highly-efficient concentrated perovskite solar cell-thermoelectric generator tandem system. J Energy Chem. 2021;59:730–735. doi: 10.1016/j.jechem.2020.12.020

[16] Liu ZY, Sun B, Zhong Y, et al. Novel integration of carbon counter electrode based perovskite solar cell with thermoelectric generator for efficient solar energy conversion. Nano Energy. 2017;38:468–476. doi: 10.1016/j.nanoen.2017.06.016

[17] Xu L, Xiong Y, Mei A, et al. Efficient perovskite photovoltaic-thermoelectric hybrid device. Adv Energy Mater. 2018;8(13). doi: 10.1002/aenm.201702937

[18] Wang N, Han L, He HC, et al. A novel high-performance photovoltaic-thermoelectric hybrid device. Energy Environ Sci. 2011;4 (9):3676–3679. doi: 10.1039/c1ee01646f